Scientific
Research
Publishing

Comparison of Different Reconstruction Algorithms for Decreasing the Exposure Dose during Digital Breast Tomosynthesis: A Phantom Study

Tsutomu Gomi

School of Allied Health Sciences, Kitasato University, Sagamihara, Japan
Email: gomi@kitasato-u.ac.jp

Abstract

We compared reconstruction algorithms [filtered back projection (FBP), maximum likelihood expectation maximization (MLEM), and the simultaneous iterative reconstruction technique (SIRT)] in terms of the radiation dose and image quality, for exploring the possibility of decreasing the radiation dose during digital breast tomosynthesis (DBT). The three algorithms were implemented using a DBT system and experimentally evaluated using measurements, such as signal difference-to-noise ratio (SDNR) and intensity profile, on a BR3D phantom (in-focus plane image). The possible radiation dose reduction, contrast improvement, and artifact reduction in DBT were evaluated using different exposure levels and the three reconstruction techniques. We performed statistical analysis (one-way analysis of variance) of the SDNR data. The effectiveness of each technique for enhancing the visibility of the BR3D phantom was quantified with regard to SDNR (FBP versus MLEM, $P < 0.05$; FBP vs. SIRT, $P < 0.05$; MLEM vs. SIRT, $P = 0.945$); the artifact reduction was quantified with regard to the intensity profile. MLEM and SIRT produced reconstructed images with SDNR values indicative of low-contrast visibility. The SDNR value for the half-radiation dose MLEM and SIRT images was close to that of the FBP reference radiation dose image. Artifacts were decreased in the MLEM and SIRT images (in the in-focus plane) according to the intensity profiles that we obtained. With MLEM and SIRT, the radiation dose may be decreased to half comparison with FBP.

1. Introduction

Tomosynthesis is a limited-angle image reconstruction method where a dataset of projections acquired at regular intervals during a single acquisition pass is used to reconstruct planar sections *post priori*. Tomosynthesis also provides the additional benefits of digital imaging [1] [2] as well as the tomographic benefits of computed tomography at decreased radiation doses and lower costs, using an approach that can easily be implemented in conjunction with radiography. Digital breast tomosynthesis (DBT) is a promising technique for improving early detection rates of breast cancer [2] [3] because it can provide three-dimensional (3D) structural information by reconstructing an entire image volume from a sequence of projection-view mammograms acquired at a small number of projection angles over a limited angular range; the total radiation dose is comparable with that used during conventional mammography screening. DBT has been shown to decrease the camouflaging effect of the overlapping fibroglandular breast tissue [4], thereby improving the conspicuity of subtle lesions. Several digital mammography-based DBT systems have been developed [5], and preliminary clinical studies are under way [2] [6].

Wu *et al*. evaluated the conventional reconstruction algorithm (filtered back projection: FBP [7]) and statistical iterative reconstruction (IR) algorithm (maximum likelihood expectation maximization: MLEM [3]). The author concluded that MLEM algorithm provided a good balance of image quality between the low and high frequency features [3]. In another report, various DBT reconstruction methods have been explored previously [7]-[9]. In fact, to date, one study has quantitatively compared DBT algorithms in terms of image quality and radiation doses [10]. In this report, IR was found to effectively decrease quantum noise and radiation exposure. However, this report was evaluated with a limited experiment [FBP vs. algebraic IR: simultaneous iterative reconstruction technique (SIRT) [11], and use of simple contrast-detail phantom].

In this study, we chose to focus on the statistical IR technique (MLEM) in addition to the algebraic IR technique (SIRT). We evaluated and compared the characteristics of the reconstructed images and the possible reduction in the radiation dose associated with MLEM, and SIRT algorithms.

2. Materials and Methods

2.1. DBT

The DBT system (Selenia Dimensions; Hologic Inc., Bedford, MA, USA) comprised an X-ray tube with a 0.3-mm focal spot (tube target: W, filtration: 0.7-mm aluminum-equivalent) and a 240×290-mm digital flat-panel amorphous selenium detector. Each detector element was 70×70 μm in size. Tomography was performed using a linear tomographic movement, with a total acquisition time 3.7 s and an acquisition angle of 15°. Projection images were sampled during a single tomographic pass (15 projections) and were used to reconstruct tomograms of a desired height. The reconstructed images (0.1 mm/pixel) were obtained at 1-mm reconstruction intervals. The distance between the source and the detector was 700 mm (**Figure 1**).
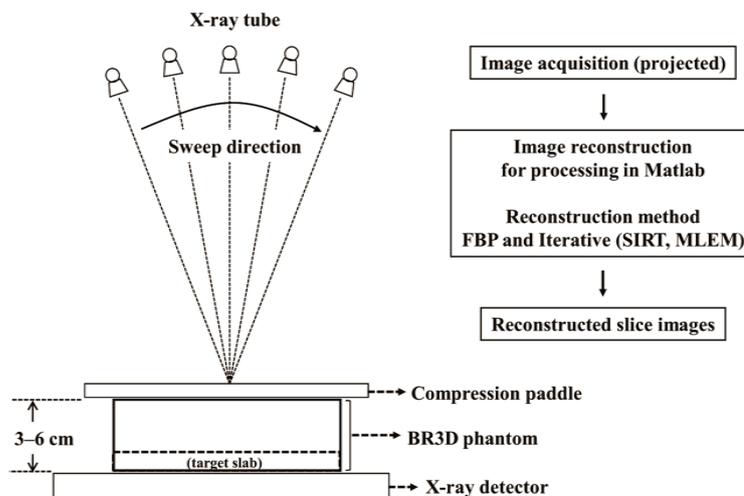
Figure 1. For tomosynthesis acquisition, the BR3D phantom was arranged parallel to the detector plane.

2.2. The Reconstruction Algorithm

Two-dimensional (2D) image filtering via multiplication of the Fourier transform by means of a Ramp or Shepp-Logan (SL) filter kernel restores the proper impulse shape for the reconstructed image. The FBP algorithm generally provides highly precise 3D reconstruction images [7]. In this study, a conventional SL filter kernel was used to reconstruct FBP images.

IR algorithms perform reconstruction recursively [8] [9], unlike the one-step operation used in back projection and FBP algorithms. Instead, reconstruction is accomplished by iteratively updating unknown linear attenuation coefficients by minimizing the error between the measured and calculated projection data.

The original method in this family of algebraic reconstruction techniques (ARTs) [11] has already been determined. ART features fast convergence speed because only a single projection value is used to update linear attenuation coefficients at a given time point, but it converges to a least-squares solution that can result in considerable noise when severely ill-posed inverse problems, such as limited-angle reconstruction, are being solved. Variations have been proposed regarding ART implementation for facilitating improvements. ART can be modified according to other methods such as SIRT, depending on the amount of projection data and the method used to update the current estimation. On the other hand, MLEM methods consisting of two steps per iteration (in which the tomosynthesis acquisition process is modeled in a forward step and the reconstructed object is updated in a backward step) have also been proposed for DBT. The most commonly studied method in DBT is MLEM introduced for DBT by Wu *et al*. [3]. MLEM and SIRT are applied iteratively such that the reconstructed volume projections, which are computed using an image formation model, resemble the experimental projections. In this study, seven MLEM and SIRT iterations were used to improve image quality (to attain highest contrast and to minimize artifacts). In this study, 7 iterations were used for image quality. The FBP, MLEM, and SIRT image reconstruction calculations from real projection data of a DBT system were performed using MATLAB (Mathworks, Natick, MA, USA) [12].

2.3. Phantom Specifications

A BR3D phantom (Model 020; CIRS Inc., Norfolk, VA, USA) consists of multiple heterogeneous slabs that mimic the glandular and adipose tissue composition and parenchymal patterns of a human breast. The slabs are made of epoxy resins with X-ray attenuation properties corresponding to 50% glandular/50% adipose breast tissue. We arranged the nontarget slabs at the top (20 - 50 mm) and bottom of the target slab (10 mm).

2.4. Measurement of the Radiation Dose

Each radiation dose setup was implemented using the following settings: a reference radiation dose [automatic exposure control (AEC) = the exposure condition at 40-mm thickness and determined tube voltage and tube current values] of 28 kVp, 50 mA; a half-radiation dose of 28 kVp, 24 mA; and a quarter-radiation dose of 28 kVp, 12 mA. All target and filter combinations contained tungsten (W) and rhodium (Rh).

We calculated the average glandular dose (AGD) according to the method suggested by Dance *et al*. [13]. We used a Piranha dosimeter for measurement of radiation exposure (RTI Electronics AB, Sweden). The purpose of the radiation dose measurement was to convert the established exposure condition (mA) into AGD (mGy). AGD results were as follows; for the reference radiation dose, thickness 30 mm: 1.78 mGy, thickness 40 mm: 1.51 mGy, thickness 50 mm: 1.29 mGy, and thickness 60 mm: 1.13 mGy; for the half-radiation dose, thickness 30 mm: 0.93 mGy, thickness 40 mm: 0.78 mGy, thickness 50 mm: 0.67 mGy, and thickness 60 mm: 0.59 mGy; and for the quarter-radiation dose, thickness 30 mm: 0.48 mGy, thickness 40 mm: 0.40 mGy, thickness 50 mm: 0.34 mGy, and thickness 60 mm: 0.30 mGy.

2.5. Evaluation

To quantitatively evaluate the quality of the reconstructed images, we evaluated the image contrast derived from the signal difference-to-noise ratio (SDNR) [14] in the in-focus plane [region of interest (ROI)-1, 6.3 mm diameter; ROI-2, 4.7 mm diameter; ROI-1 and ROI-2 have the same region size: spheroidal masses (epoxy resin)]. The SDNR is often used in tomosynthesis imaging for estimation of low-contrast detectability. SDNR was defined as follows:

$$SDNR = \frac{\left|\mu_{\text{Feature}} - \mu_{BG}\right|}{\left(\sigma_{\text{Feature}} + \sigma_{BG}\right)/2}$$

where μ_{Feature} is the mean object pixel value, μ_{BG} is the mean background area pixel value, σ_{Feature} is the standard deviation of the object pixel values, and σ_{BG} is the standard deviation of the background pixel values. The parameter σ_{BG} not only includes the photon statistics and electronic noise from the results but also the structural noise that might obscure the object. The sizes of all ROIs were adjusted to a signal internally. ROI areas (44 pixels) for measurement of SDNR are presented in **Figure 2**.

To evaluate the quality of the reconstructed image, we constructed the image artifacts derived from the intensity profiles. Different reconstruction methods in the in-focus plane were used to compare intensity profiles for the evaluation of the microcalcification sites (0.4 mm φ; $CaCO_3$). Intensity areas for measurement of the profile data are presented in **Figure 2**.
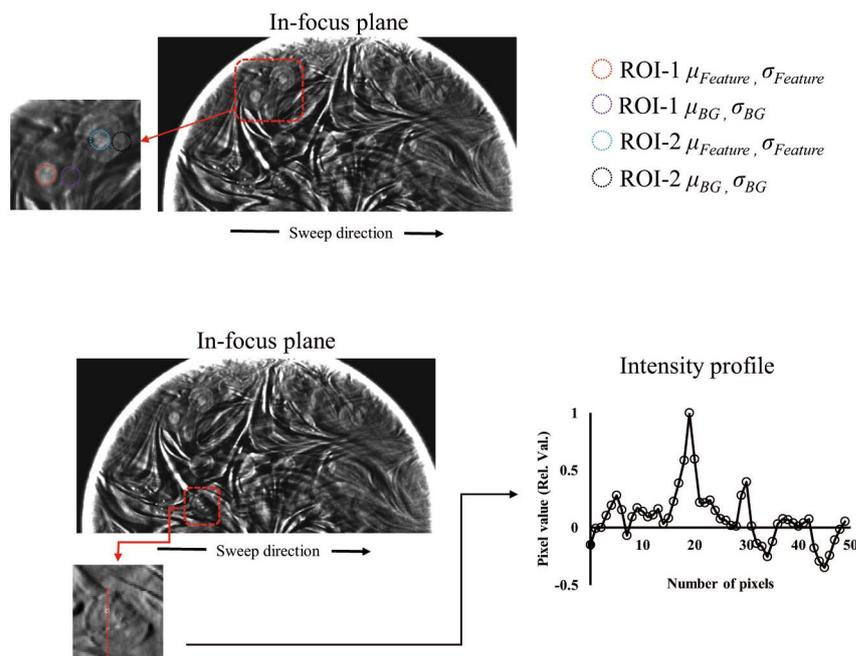
The effects of image contrast were assessed in one-way analysis of variance and multiple comparison (the Tukey–Kramer test). Statistical tests were used to assess differences between SDNR values of FBP, MLEM, and SIRT. We performed the tests on a total of 72 samples (FBP: 24, MLEM: 24, SIRT: 24). The statistical analysis was performed in SPSS for Windows, version 21.0 (SPSS Inc., Chicago, IL, USA). All probability (P) values < 0.05 were assumed to denote statistical significance.

3. Results

The results revealed that MLEM and SIRT produced reconstructed images with features (6.3 mm φ and 4.7 mm φ, respectively) with no artifacts in the horizontal direction (the X-ray sweep direction). Review of the results revealed that both DBT artifact reduction and image contrast were most effective with MLEM and SIRT at all radiation dose levels (**Figure 3**).

The image contrast and different-diameter characteristics yielded equivalent SDNRs (in the in-focus plane) for MLEM and SIRT. With FBP, the detectability rates for the reference radiation dose in the SDNR experiment were approximately equivalent to those of the image contrast and different-diameter characteristic half-radiation dose images generated using MLEM and SIRT (**Figure 4**).

We show results of one-way analysis of variance in **Table 1**. The difference in image contrast between FBP (mean ± mean squared error, 1.53 ± 0.11) and MLEM (mean ± mean squared error, 3.46 ± 0.20) was statistically

In-focus plane

ROI-1 $\mu_{Feature}$, $\sigma_{Feature}$
ROI-1 μ_{BG}, σ_{BG}
ROI-2 $\mu_{Feature}$, $\sigma_{Feature}$
ROI-2 μ_{BG}, σ_{BG}

Sweep direction

In-focus plane

Intensity profile

Sweep direction

Figure 2. Areas of measurement of the signal difference-to-noise ratio (SDNR) and intensity profile metrics (the image shown: a reconstructed image of the BR3D phantom [in-focus plane]).
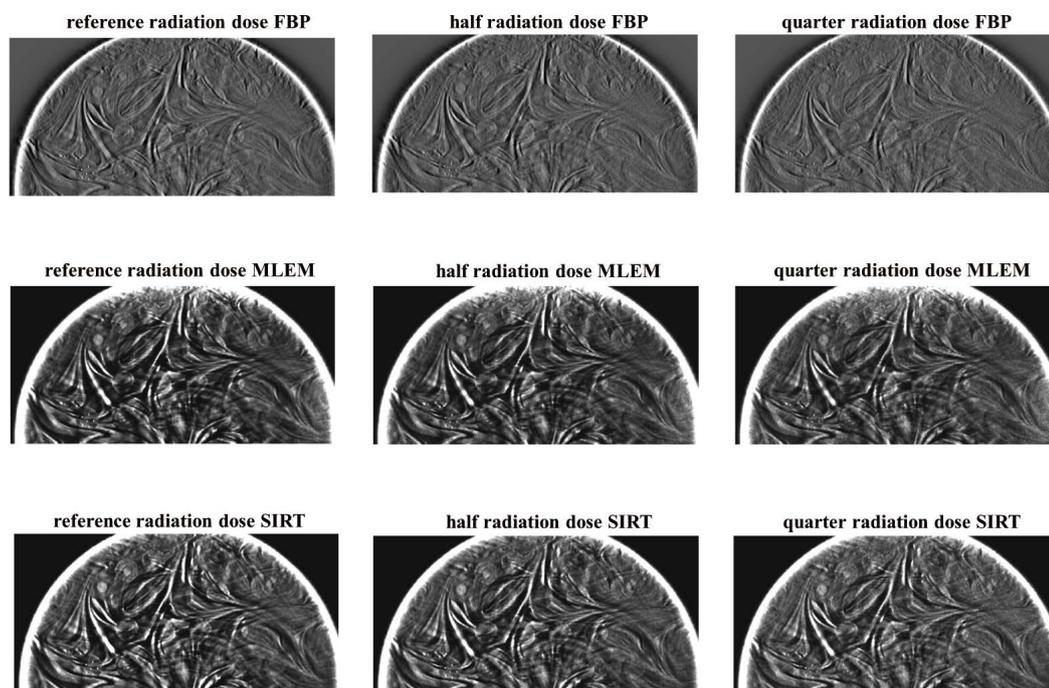
Figure 3. Comparison of digital breast tomosynthesis images and images obtained using the following reconstruction algorithms: filtered back projection (FBP), maximum likelihood expectation maximization (MLEM), and the simultaneous iterative reconstruction technique (SIRT) in the in-focus plane (phantom thickness: 40 mm).
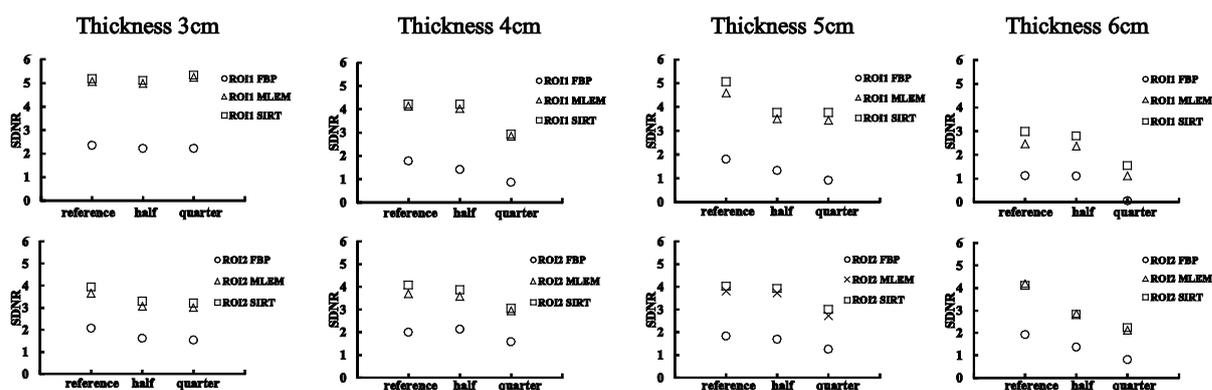
Figure 4. Comparison of the signal difference-to-noise ratio (SDNR) values obtained using digital breast tomosynthesis in the in-focus plane [region of interest (ROI)-1, 6.3 mm φ; ROI-2, 4.7 mm φ; spheroidal masses (epoxy resin)] for different values of phantom thickness and radiation exposure. Maximum likelihood expectation maximization (MLEM) and the simultaneous iterative reconstruction technique (SIRT) were used. The contrast detectability obtained by means of these techniques was higher than that obtained with the filtered back projection (FBP) technique.

Table 1. Results of one-way analysis of variance.

Source of variation	df	Sums of squares	Mean square	F	P
Group	2	66.661	33.331	46.196	<0.05
Error	69	49.784	0.722	-	-

df: Degree of freedom.

significant [$P < 0.05$, difference: 1.92, 95% confidence interval (CI): −2.61 to −1.22]. The difference in image contrast between FBP and SIRT (mean ± mean squared error, 3.68 ± 0.19) was also statistically significant [$P < 0.05$, difference: 2.14, 95% CI: −2.83 to −1.44]. The difference in image contrast between MLEM and SIRT was
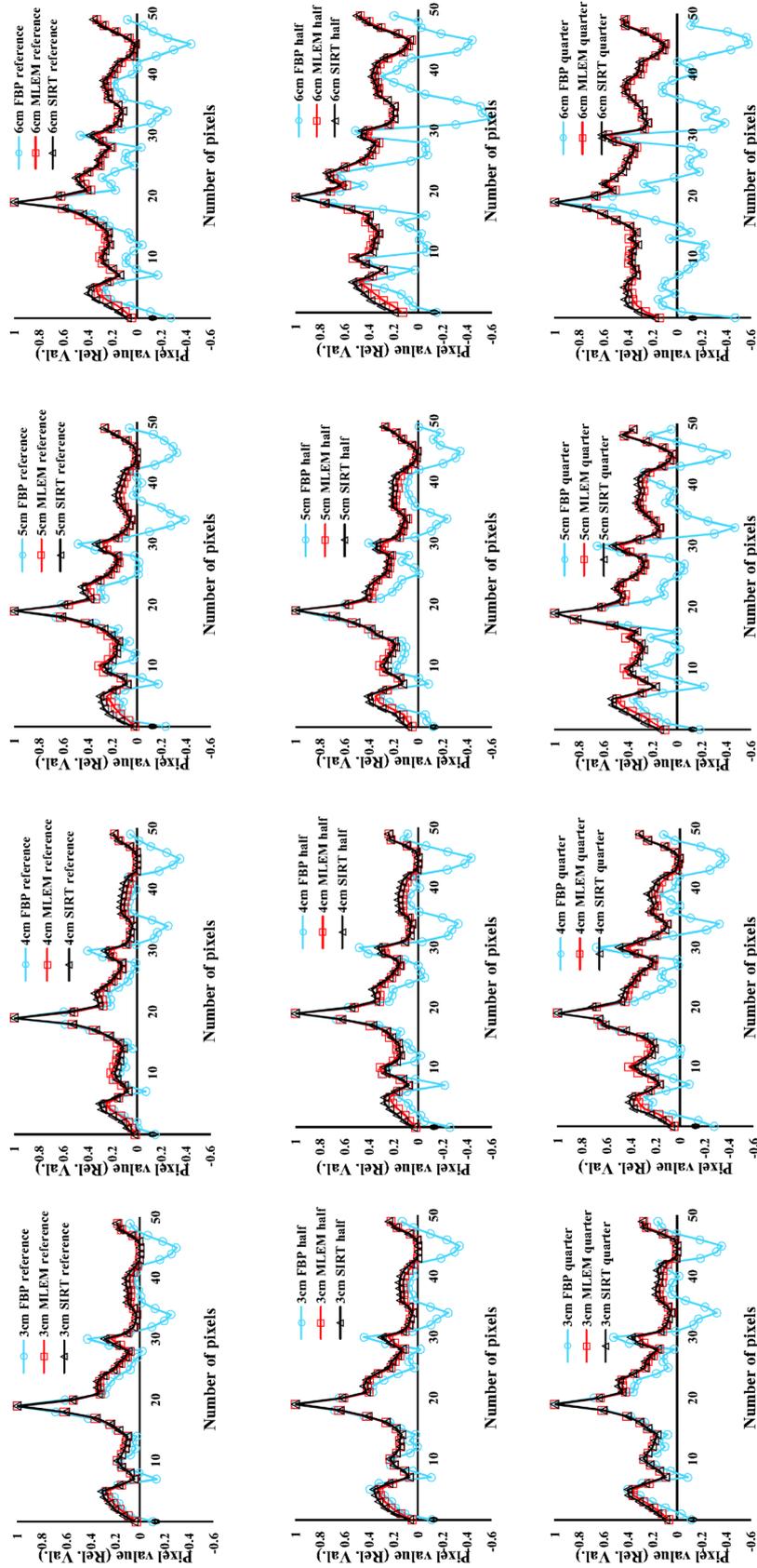
Figure 5. Comparison of the intensity profiles obtained using digital breast tomosynthesis in the in-focus plane [microcalcification sites, 0.4 mm φ; CaCO$_3$] for different values of phantom thickness and radiation exposure. Maximum likelihood expectation maximization (MLEM) and the simultaneous iterative reconstruction technique (SIRT) were used; the artifacts formed with these techniques were less noticeable than those formed with the filtered back projection (FBP) technique.

476

not statistically significant ($P = 0.945$, difference: 0.21, 95% CI: −0.91 to 0.47).

The intensity profiles of FBP, MLEM, and SIRT images are presented in **Figure 5**. Artifacts were decreased with MLEM and SIRT, and the consequent improvements in image quality (related to the signal undershooting) were demonstrated. Better image quality in terms of artifact reduction was demonstrated with MLEM and SIRT than FBP.

Comparison of SDNRs at different radiation doses revealed that the improved results required exposure above that of a half-radiation dose because the SDNR value for the half-radiation dose MLEM and SIRT images was close to that of the FBP reference radiation dose image. We assessed the likelihood of decreasing the radiation dose to quarter until thickness 60 mm when using MLEM and SIRT with comparison FBP reference radiation dose image. The artificial image tended to need enlargement when the radiation dose was decreased to quarter (**Figure 5**). This result suggested that the MLEM and SIRT radiation dose could be decreased by half for the thickness 30 - 60 mm.

4. Discussion

Our empirical results clearly demonstrate feasibility of the radiation dose reduction to half for low-radiation dose DBT images using the MLEM and SIRT methods that we tested. For example, the efficiency of this technique may be quantitatively assessed on the basis of intensity profiles and SDNR, which are presented in **Figure 3** and **Figure 4**. In the SDNR experiment, the detectable contrast in the FBP reference radiation dose images and half-radiation dose images obtained using MLEM and SIRT were approximately equivalent; therefore, this technique may help to decrease the DBT radiation dose.

SIRT does not imply even distribution of noise across the entire image. Instead, an algebraic matrix is used to selectively identify and then subtract noise from the image according to a mathematical model. The objective with MLEM (statistical method) is to identify the reconstructed image that maximizes the likelihood of having observed the particular projection measurements [15]. In the MLEM algorithm, because high-frequency noise in the data is amplified by each iteration of the reconstruction algorithm, a smaller number of iterations may be optimal for detection of low-contrast objects, such as small tumors [3]. In the comparison of FBP and MLEM, the latter showed a good balance of image quality between the low-frequency and high-frequency features [3]. The result is a less noisy image, which is an unexpected effect of artifact reduction in the image.

In general, the observed artifacts in an image are caused by the loss of the largest normal contributions from artifact-free voxels. These voxels yield normal original contributions, and their values are slightly decreased after the largest normal contribution is omitted. A voxel with a single abnormal contribution is relieved of this contribution while retaining all other contributions, including the largest normal contribution. Therefore, these voxels tend to exhibit higher values than their neighboring artifact-free voxels, leading to the appearance of objects in which artifact-free voxels are more noticeable against the background. This phenomenon is a drawback of the FBP technique, but artifacts due to this effect are very conspicuous when such images are compared with artifact-free images.

There are some limitations to our phantom study. The materials constituting the BR3D phantom were only simulations of the mammary gland, and we did not test real mammary-gland tissues. On the other hand, we believe that the consistency of the BR3D phantom means that it is an accurate representation of real mammary-gland tissue. Despite the limitations, we believe that our results can serve as reference data when physicians consider decreasing radiation exposure.

5. Conclusion

In conclusion, our empirical results demonstrate that MLEM and SIRT can be used to improve image contrast by suppressing streak artifacts in DBT images obtained using both reference and half-radiation doses. With MLEM and SIRT, the radiation levels may be decreased by 50% relative to the FBP technique. IR may yield improvements in image quality and a reduction in the radiation dose in comparison with the conventional FBP technique.

References

[1]   Sone, S., Kasuga, T., Sakai, F., Kawai, T., Oguchi, K., Hirano, H., Li, F., Kubo, K., Honda, T., Hniuda, M., Takemura, K. and Hosoba, M. (1995) Image Processing in the Digital Tomosynthesis for Pulmonary Imaging. *European Radiology*,

5, 96-101.

[2] Skaane, P., Bandos, A.I., Gullien, R., Eben, E.B., Ekseth, U., Haakenaasen, U., Izadi, M., Jebsen, I.N., Jahr, G., Krager, M., Niklason, L.T., Hofvind, S. and Gur, D. (2013) Comparison of Digital Mammography Alone and Digital Mammography plus Tomosynthesis in a Population-Based Screening Program. *Radiology*, **267**, 47-56. http://dx.doi.org/10.1148/radiol.12121373

[3] Wu, T., Stewart, A., Stanton, M., McCauley, T., Phillips, W., Kopans, D.B., Moore, R.H., Eberhard, J.W., Opsahl-Ong, B., Niklason, L. and Williams, M.B. (2003) Tomographic Mammography Using a Limited Number of Low-Dose Cone-Beam Projection Images. *Medical Physics*, **30**, 365-380. http://dx.doi.org/10.1118/1.1543934

[4] Helvie, M.A., Roubidoux, M.A., Zhang, Y., Carson, P.L. and Chan, H.P. (2006) Tomosynthesis Mammography vs. Conventional Mammography: Lesion Detection and Reader Reference. Initial Experience. *RSNA Program Book*, 335.

[5] Sechopoulos, I., Bliznakova, K. and Fei, B. (2013) Power Spectrum Analysis of the X-Ray Scatter Signal in Mammography and Breast Tomosynthesis Projections. *Medical Physics*, **40**, 101905-1-101905-7. http://dx.doi.org/10.1118/1.4820442

[6] Gur, D., Zuley, M.L., Anello, M.I., Rathfon, G.Y., Chough, D.M., Ganott, M.A., Hakim, C.M., Wallace, L., Lu, A. and Bandos, A.I. (2012) Dose Reduction in Digital Breast Tomosynthesis (DBT) Screening Using Synthetically Reconstruction Projection Images: An Observer Performance Study. *Academic Radiology*, **19**, 166-171. http://dx.doi.org/10.1016/j.acra.2011.10.003

[7] Dobbins 3rd, J.T. and Godfrey, D.J. (2003) Digital X-Ray Tomosynthesis: Current State of the Art and Clinical Potential. *Physics in Medicine and Biology*, **48**, R65-R106. http://dx.doi.org/10.1088/0031-9155/48/19/R01

[8] Bleuet, P., Guillemaud, R., Magnin, I. and Desbat, L. (2001) An Adapted Fan Volume Sampling Scheme for 3D Algebraic Reconstruction in Linear Tomosynthesis. *IEEE Transactions on Nuclear Science*, **3**, 1720-1724.

[9] Wu, T., Zhang, J., Moore, R., Rafferty, E. and Kopans, D. (2004) Digital Tomosynthesis Mammography Using a Parallel Maximum-Likelihood Reconstruction Method. *Proceedings of SPIE*, **5368**, 1-11. http://dx.doi.org/10.1117/12.534446

[10] Gomi, T. (2014) A Comparison of Reconstruction Algorithms regarding Exposure Dose Reductions during Digital Breast Tomosynthesis. *Journal of Biomedical Science and Engineering*, **7**, 516-525. http://dx.doi.org/10.4236/jbise.2014.78053

[11] Gordon, R., Bender, R. and Hermen, G.T. (1970) Algebraic Reconstruction Techniques (ART) for Three-Dimensional Electron Microscopy and X-Ray Photography. *Journal of Theoretical Biology*, **29**, 471-481. http://dx.doi.org/10.1016/0022-5193(70)90109-8

[12] Mathworks Inc. (2014) http://www.mathworks.com/products/matlab/

[13] Dance, D.R., Young, K.C. and van Engen, R.E. (2011) Estimation of Mean Glandular Dose for Breast Tomosynthesis: Factors for Use with the UK, European and IAEA Breast Dosimetry Protocols. *Physics in Medicine and Biology*, **56**, 453-471. http://dx.doi.org/10.1088/0031-9155/56/2/011

[14] Li, K., Ge, Y., Garrett, J., Bevins, N., Zambelli, J. and Chen, G.H. (2014) Grating-Based Phase Contrast Tomosynthesis Imaging: Proof-of-Concept Experimental Studies. *Medical Physics*, **41**, 011903-1-011903-11. http://dx.doi.org/10.1118/1.4835455

[15] Das, M., Gifford, H.C., O'Connor, J.M. and Glick, S.J. (2011) Penalized Maximum Likelihood Reconstruction for Improved Microcalcification Detection in Breast Tomosynthesis. *IEEE Transactions on Medical Imaging*, **30**, 904-914. http://dx.doi.org/10.1109/TMI.2010.2089694

Abbreviations

DBT Digital breast tomosynthesis
FBP Filtered backprojection
MLEM Maximum likelihood expectation maximization
SIRT Simultaneous iterative reconstruction technique
SDNR Signal difference-to-noise ratio